

# Low-frequency sea-level variability in the South China Sea and its relationship to ENSO

Guoqi Han · Weigen Huang

Received: 1 April 2008 / Accepted: 4 October 2008 / Published online: 6 November 2008  
© Springer-Verlag 2008

**Abstract** Sea-level variability in the South China Sea was investigated based on satellite altimetry, tide-gauge data, and temperature and salinity climatology. The altimetric sea-level results clearly reveal three distinct amphidromes associated with the annual cycle. The annual sea level is higher in fall/winter in the coast and shelf region and lower in summer/fall in the central sea, agreeing well with independent tide-gauge data. Averaged over the deep basin (bottom depth > 2,000 m), the annual cycle can be approximately accounted for by the steric height relative to 700 db. Significant interannual sea-level change is observed from altimetry and tide-gauge data. The interannual and longer-term sea-level variability in the altimetric data is negatively correlated (significant at the 95% confidence level) with the El Niño - Southern Oscillation (ENSO), attributed in part to the steric height change. The altimetric sea-level rise rate is 1.0 cm/year for the period from 1993 to 2001, which is consistent with the rate derived from coastal tide-gauge data and approximately accountable for by the steric height calculated relative to 700 db. The tide-gauge sea-level (steric height) rise rate of 1.05 (0.9) cm/year from 1993 to 2001 is much larger than that of 0.22 (0.12) cm/year for the period from 1979 to 2001, implying the sensitivity to the length of data as a result of the decadal variability. Potential roles of the ENSO in the interannual

and longer-term sea-level variability are discussed in terms of regional manifestations such as the ocean temperature and salinity.

## 1 Introduction

Circulation in the South China Sea (SCS) is characterized by a cyclonic gyre in winter (Chu et al. 1998; Qu 2000) and an anticyclonic gyre in the southern SCS and a cyclonic gyre in the northern SCS in summer (Wang et al. 2003), primarily in response to seasonally reversing monsoon. On the interannual scale, the circulation may be modulated by the El Niño-Southern Oscillation (ENSO) (e.g., Wu and Chang 2005; Fang et al. 2006). The intrusion of the Pacific water through Luzon Strait may have important impacts as well (Qu 2000).

Seasonal sea-level and circulation variations in the SCS have been extensively studied using hydrographic data (e.g., Qu 2000), ocean models (e.g., Shaw and Chao 1994; Chu et al. 1998), and satellite altimetry (e.g., Morimoto et al. 2000). Previous studies indicate that the annual sea-level cycle in the SCS is mainly forced by seasonal reversing monsoon (e.g., Qu 2000; Shaw et al. 1999). Mesoscale eddies also have evident seasonality (Wang et al. 2003), for example, the development of the dipole structure off central Vietnam in summer (Wang et al. 2006b) and the formation of alternating eddies in the eastern SCS in winter (Qu 2000; Wang et al. 2008). Zhang et al. (2006) used 2-year (2004–2005) merged altimeter data to examine annual amphidromes. They attempted to explain dynamical mechanisms of the annual sea-level amphidromes by making an empirical orthogonal function (EOF) analysis of the 2004–2005 altimetric sea-level anomalies, suggesting that the existence of the amphidromes is a consequence of the unique seasonal

---

G. Han (✉)  
Fisheries and Oceans Canada,  
Northwest Atlantic Fisheries Centre,  
St. John's, NL A1C 5X1, Canada  
e-mail: guoqi.han@dfo-mpo.gc.ca

W. Huang  
State Key Laboratory of Satellite Ocean Environment Dynamics,  
Second Institute of Oceanography, State Oceanic Administration,  
Hangzhou, China

sea-level variation in the vicinity of the Vietnam eddy. Clearly, their results are limited by the interference of the unresolved interannual fluctuations, which are evidently present in their extracted first and second EOF modes.

Interannual and decadal variability and long-term sea-level changes in the SCS have become a heated subject in recent years. Using a data assimilative model and EOF analysis, Wu and Chang (2005) illustrated two distinct anomaly patterns in the SCS, which had strong interannual variations and were highly correlated with ENSO events. A secular sea-level trend of  $6.7 \pm 2.7$  mm/year was found to be much larger than the corresponding global rate, and interannual sea-level variation to be correlated with the Niño 3.4 index (Fang et al. 2006). On the global scale, tide-gauge data indicated a mean sea-level rise of 1–2 mm/year during the last century (Church et al. 2001); while satellite altimetry showed a drastic acceleration of the sea-level rise during 1993–2003 ( $2.8 \pm 0.4$  mm/year; Cazenave and Nerem 2004). It is not clear if the latter simply represents the decadal variability. Significant regional contrasts in the sea-level change have been reported (Cazenave and Nerem 2004; Han 2004), related to characteristic large-scale variability and regional manifestation. Wang et al. (2006a) from an analysis of global ocean model results indicated the SCS upper-layer circulation was closely correlated with El Niño from 1981–2004. The SCS sea level based on satellite altimetry rose from 1993 to 2001 and fell afterwards (Fang et al. 2006). Chang et al. (2008) demonstrated the roles of ENSO in the SCS summer circulation.

In the aforementioned SCS studies, tide-gauge data were rarely used to verify or complement the hydrography-, model-, and altimetry-based analyses. The potential effect of the tidal correction error on the altimetry-derived seasonal variability or the sensitivity of the interannual variability and secular trend to the short record of altimetry was not sufficiently discussed. In this study we investigate seasonal, interannual, and long-term sea-level changes from merged satellite altimetric measurements, tide-gauge observations, and hydrographic data in the SCS and explore potential roles of ENSO in these changes. Annual harmonics of sea-level variation and residual tides are extracted from altimetric sea-surface heights using a modified response-analysis method. The residual sea levels are averaged by season and year for interannual variability and trend detection. The modified response-analysis method is able to well separate the annual cycle from the aliases tidal error. The sensitivity of the decadal variability and secular trend to the length of data is discussed.

The paper has five sections. Section 2 describes the methodology of processing and analyzing satellite altimetry measurements, tide-gauge data, and temperature and salinity data. Section 3 presents and interprets the annual sea-level cycle. Section 4 presents the interannual and longer-term sea-

level variability and its possible relationship with the ENSO, temperature, and salinity is discussed. Section 5 concludes the paper.

## 2 Methodology

### 2.1 Altimeter data processing and analysis techniques

We have used weekly merged sea-surface height anomalies from AVISO. The dataset is an objectively mapped product of TOPEX/Poseidon, ERS-1, ERS-2, Geosat-Follow-on and Envisat altimeter data, with a  $1/3^\circ$  Mercator projection grid (Ducet et al. 2000). The zonal and meridional spacing for each grid is identical and varies with the latitude. Therefore the spatial resolution increases with latitude. All standard corrections were made to account for atmospheric (wet troposphere, dry troposphere, and ionosphere delays) and oceanographic (electromagnetic bias; ocean, load, solid Earth and pole tides) effects. The data duration is from 1992 to 2006.

We apply a modified response-analysis method (e.g., Han et al. 2002) to the sea-surface height anomalies to separate the annual cycle from variations at alias frequencies of oceanic tides. In this method, the sea-level anomalies ( $\zeta$ ) are expressed as

$$\zeta(\varphi, \lambda, t) = \sum_{m=1}^2 \sum_{k=0}^{2K} [\overline{U}_k^m(\varphi, \lambda) P_k^m(t) + \overline{V}_k^m(\varphi, \lambda) Q_k^m(t)] + C \cos \omega t + S \sin \omega t + r \quad (1)$$

where  $\varphi$  and  $\lambda$  are longitude and latitude;  $t$  is the time;  $m$  denotes the tidal species (1 for the diurnal and 2 for the semi-diurnal);  $k$  is time lag in days ( $K=1$  is adequate);  $\overline{U}_k^m$  and  $\overline{V}_k^m$  are unknowns to be determined, from which amplitudes and phases for the diurnal and semi-diurnal can be obtained;  $P_k^m$  and  $Q_k^m$  are nearly orthogonal in time, associated with the real and imaginary parts of the time-varying portion of the tide-generating potential;  $C$  and  $S$  are cosine and sine coefficients for the annual cycle that are to be determined;  $\omega$  is the annual frequency; and  $r$  is the residual sea-level anomalies. A least-squares technique is used to solve Eq. (1). The residual sea-level anomalies are further analyzed to examine the interannual variability and the sea-level rise.

The modified response method is applied to the initially corrected altimetric sea-surface height anomalies to extract the annual cycle and to remove the remaining variability of major semidiurnal ( $M_2$ ,  $S_2$ ,  $N_2$ ,  $K_2$ ) and diurnal ( $K_1$ ,  $O_1$ ,  $P_1$  and  $Q_1$ ) tides. With the repeat cycle of approximately 10 days for the T/P altimeter, semi-diurnal and diurnal tides

in the T/P data have much longer alias periods (Han et al. 1996) but all less than half a year, for example, 62 days for  $M_2$ . Therefore, any tidal correction errors are not a concern to the present investigation of the annual, interannual, and long-term variability, given the data record of well over a decade.

## 2.2 Tide-gauge data

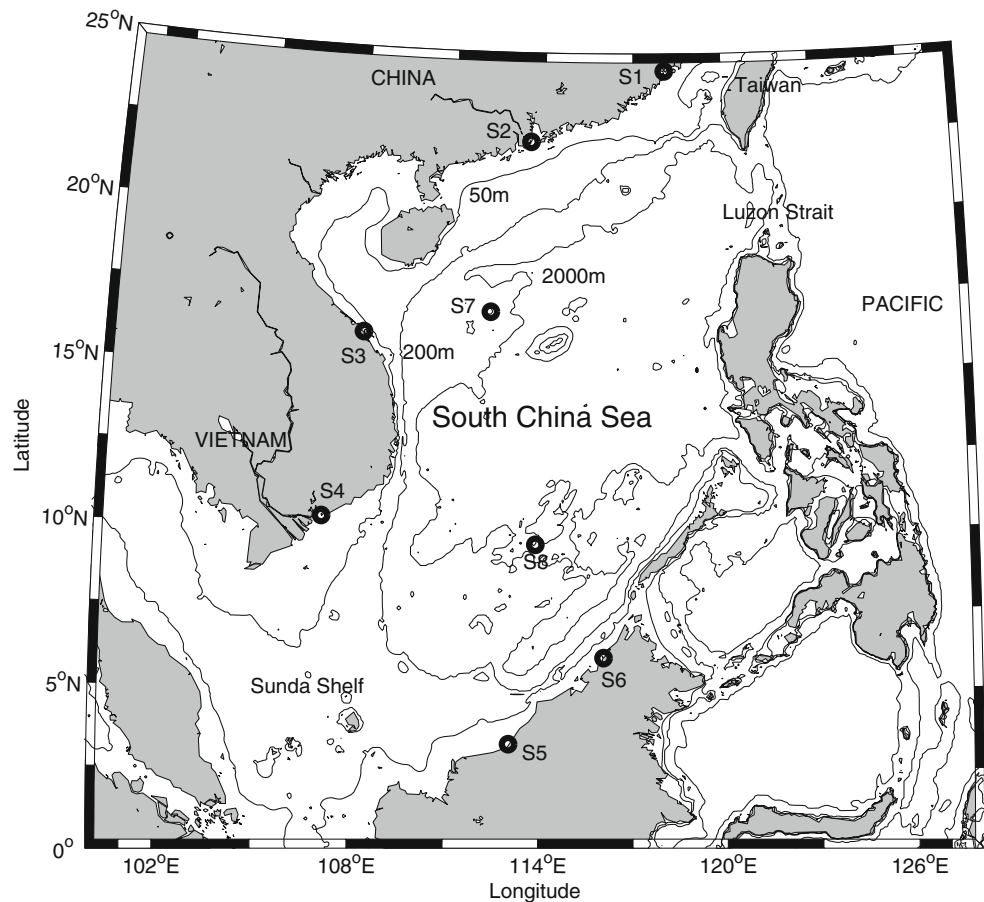
We obtain monthly-mean sea-level data of eight tide-gauge stations (see Fig. 1 for locations) from the Permanent Service for Mean Sea Level (PSMSL) (<http://www.pol.ac.uk/psmsl>). The data duration varies significantly from station to station and is usually about 10 years or more, starting as early as 1900s and ending as late as 2004. For the annual cycle, we use monthly sea-level data from 1993 to 2001. For longer-term sea-level variability and rise, we use monthly sea-level data at five selected sites (S1, S3, S5, S6, and S7) from 1979 or 1993 to 2001. The monthly sea-level data are corrected for the inverse barometric effect. Although the inverse barometric response of the sea level may not be perfect, on the seasonal and longer time scales the assumption is reasonably good and robust (Han et al. 1993).

Monthly-mean sea-level anomalies are computed by removing the means from the sea-level data for each station. A least-squares analysis is performed to extract annual and semiannual cycles from the monthly anomalies. For stations S1, S3, S5, S6, and S7, the residual monthly data with the annual and semiannual cycles removed are then used to generate seasonal-mean (January–March for winter, April–June for spring, July–September for summer and October–December for fall) sea-level anomalies. A least-squares regression was used to extract the linear trend (the sea-level rise rate).

## 2.3 Temperature and salinity climatology and steric height

Ishii et al.'s (2006) monthly-mean temperature and salinity data sets are used to calculate the steric height at selected locations in the study region. The Ishii et al.'s fields were objectively analyzed on a  $1 \times 1^\circ$  grid at the upper 16 standard levels (the deepest level is 700 m) for 1945–2003. They used various historical hydrographic datasets, which include the latest version of the observational data, climatology, and standard deviations compiled by the National Oceanic and Atmospheric Administration/National Oceanographic Data Center (NODC). In addition, Ishii et al.'s

**Fig. 1** South China Sea and its vicinity. Open circles are the locations of coastal tide-gauge stations. The 50-, 200-, and 2,000-m isobaths are also shown



(2006) climatology included a tropical and subtropical Pacific Ocean sea-surface salinity dataset for 1970–2001 and a global database archived by the Global Temperature-Salinity Profile Program of NODC from 1990 to 2003, with the drop rate correction for the XBT data applied.

We have calculated the steric height relative to 700 db based on the temperature and salinity climatology. Steric height anomalies are computed by removing the temporal mean for each location.

### 3 Annual cycle

#### 3.1 Annual sea-level pattern

The least-squares analysis extracts the annual cycle of sea level from the altimetric data from 1992–2006. In this section, we examine the amplitude and phase of the annual cycle of altimetric sea levels and compare the altimetric results with coastal tide-gauge measurements and steric heights calculated from Ishii et al.'s (2006) temperature and salinity climatology.

There is significant spatial variability in the amplitude of the altimetric annual cycle, from nearly zero in the vicinity of amphidromic points to over 20 cm along some of the coastal and shelf seas (Fig. 2). The phase (the time of annual maximum sea level) pattern indicates that the annual sea level along the coastal and shelf seas is higher in fall/winter; while the sea level in the central basin is higher in summer/fall. We have interpolated the altimeter results onto eight tide-gauge locations. A comparison of the T/P annual cycle with tide-gauge measurements indicates overall good

agreement (Table 1). There are some larger discrepancies off the Vietnam coast where the sea-level changes sharply toward the coast and in the vicinity of the amphidromes where the annual amplitude is very small. Statistically, the correlation coefficient for amplitude is 0.98. The mean and root-mean-square (RMS) amplitude differences (altimetry minus tide-gauge) are  $-2.4 \pm 1.3$  cm and 2.7 cm, respectively, relatively small compared to the RMS amplitude of 14.5 cm based on tide-gauge observations. The correlation coefficient for phase is 1.00. The mean and RMS phase differences are  $13 \pm 8$  d and 15 d, respectively.

We have calculated the steric height relative to 700 db (Fig. 3) based on Ishii et al.'s (2006) temperature and salinity climatology. On average, the annual cycle of the steric height has an amplitude of 4.5 cm and peaks in August, close to the altimetric results averaged over the deep SCS (bottom depth > 2,000 m). Therefore, on the basin scale, the annual sea-level change in the deep SCS seems to be mainly associated with the temperature and salinity variation. However, there are substantial differences in the spatial distribution between the altimetric and steric results. The steric height pattern suggests two amphidromes, which, however, are not as clearly defined as those in the altimetric results. The discrepancies can in part be ascribed to the low spatial resolution of the temperature and salinity data.

#### 3.2 Annual amphidromes

Hereinafter, we will focus on the altimetric results to discuss the annual sea-level amphidromes. Overall, the amplitude-phase pattern (Fig. 2a and b) from the present altimetric data analysis shows some qualitative and quan-

**Fig. 2** Annual harmonics of sea level from altimeter data. The amplitude contour intervals (a) are 1 cm. The phase (b) indicates the time (year day) when the annual sea level is highest. Three amphidromes A, B, and C are depicted as open circles

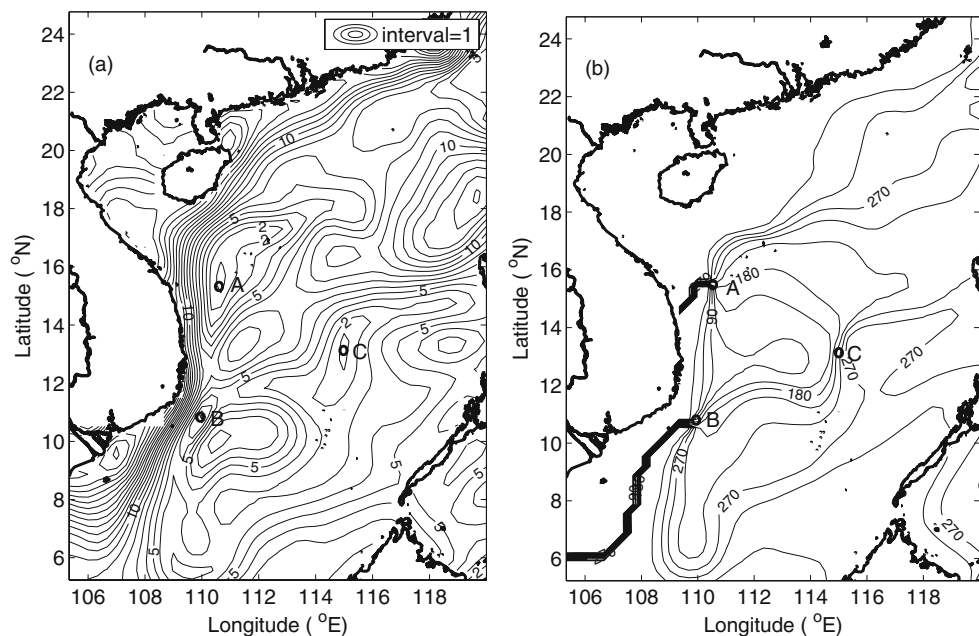


**Table 1** Comparison of the T/P and tide-gauge (braced values) sea-level annual cycle at selected tide-gauge locations (also refer to Fig. 1)

| Location           | Amplitude (cm) | Year Day  |
|--------------------|----------------|-----------|
| Xisha (S7)         | 1.8 (5.0)      | (226) 225 |
| Nansha (S8)        | 2.9 (6.5)      | 264 (239) |
| Bintulu (S5)       | 7.9 (8.5)      | 345 (341) |
| Kota Kinabalu (S6) | 6.0 (7.9)      | 318 (301) |
| Vungtau (S4)       | 20.8 (22.0)    | 12 (0)    |
| Danang (S3)        | 18.5 (22.7)    | 356 (343) |
| Xiamen (S1)        | 14.5 (17.5)    | 343 (332) |
| Macau (S2)         | 11.9 (13.4)    | 347 (327) |

The year day indicates the time when the annual sea level is highest

titative differences from Zhang et al.'s (2006). There are clearly only three annual amphidromes: two well defined (A and B) and one less well defined (C). A and B are located in the western SCS and C is located in the central SCS (Table 2). A cyclonic rotation is associated with A and an anticyclonic rotation is associated with B. Unlike Zhang et al.'s (2006), no other ill-defined amphidromes are seen in Fig. 2. An earlier study by Yanagi et al. (1997) indicated two amphidromes: one is essentially located at A and the other is about 1° south of B.

Zhang et al.'s (2006) analysis was carried out for 1-year data, separately for 2004 and 2005. They reported four highly unstable amphidromes, with numerous ill-defined ones each year. We obtain similar results (not shown) from an analysis of 2004 or 2005 data only. Given the strong interannual variability in the regional sea level, substantial semiannual and intra-seasonal variability (Fig. 4), the yearly analysis cannot achieve statistically stable results for the annual cycle, especially for the

identification of amphidromes. Therefore, the apparent high instability of amphidromic locations in the yearly analysis is not physical features but rather artifacts due to the short data length.

Now we examine the sensitivity of the extracted annual cycle (especially the amphidromes) to the time period and the data length used in the analysis. The interannual sea-level variability in the SCS seems to be dominated by ENSO frequencies at periods of 2–7 years (Fig. 4). To reduce artifacts in the annual cycle patterns, it is appropriate to use at least 7 years of data in the least-square analysis. Therefore, we have divided the entire data set into two non-overlapping segments from 1992–1999 and 1999–2006, each with about 7 years of data. Both analyses show the two primary well-defined amphidromes (A and B) in the northwest SCS and the one less well defined one (C) in the central SCS, consistent with the baseline analysis based on 14 years of data. The location of A changes within 1° or so, similar to Chen and Quartly's (2005) results for the annual sea-level amphidromes in the tropical ocean. For amphidromes B and C, the present analyses indicate they are essentially stationary given the spatial resolution of data (1/3°).

To elucidate processes associated with the annual amphidromes, we have carried out an EOF analysis of the extracted annual cycle. We choose not to analyze directly the satellite sea-level anomalies so that the EOF patterns would not be obscured by any interannual variability. Our analysis of the annual cycle shows that the first EOF mode (accounting for 74% of the total annual variability) (Fig. 5a and b) represents the basin-scale circulation anomaly in the SCS. The second EOF mode (accounting for 21% of the total annual variability) (Fig. 5c and d) represents the dipole eddy off Vietnam in summer (Wang et al. 2006b) and the

**Fig. 3** Same as Fig. 2 but for steric height based on Ishii et al.' (2006) 1 × 1° temperature and salinity climatology

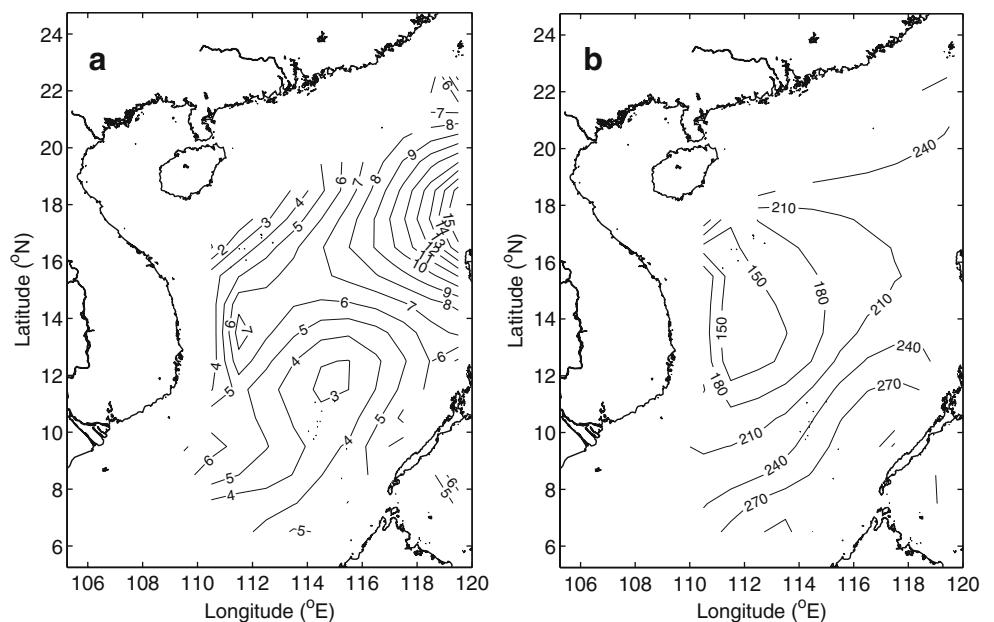




**Table 2** Locations (longitude ( $^{\circ}$ E), latitude ( $^{\circ}$ N)) of annual sea-level amphidromes in the SCS for the entire length of data (1992–2006), for 1992–1999, and for 1999–2006, respectively

|           | A           | B           | C         |
|-----------|-------------|-------------|-----------|
| Baseline  | 110.6, 15.4 | 110, 10.8   | 115, 13.1 |
| 1992–1999 | 110.5, 15.1 | 109.8, 10.6 | 115, 12.8 |
| 1999–2006 | 110.9, 16   | 110, 10.8   | 115, 12.9 |

West Luzon eddy in winter (Qu 2000; Wang et al. 2008). All three amphidromes identified in the present analysis are located on the zero contour lines of the first and second modes (Fig. 5a and c). They are located where both the dominant basin-scale and the secondary mesoscale features have nil sea-level variation. Therefore, the annual amphidromes are clearly the consequence of the unique spatial

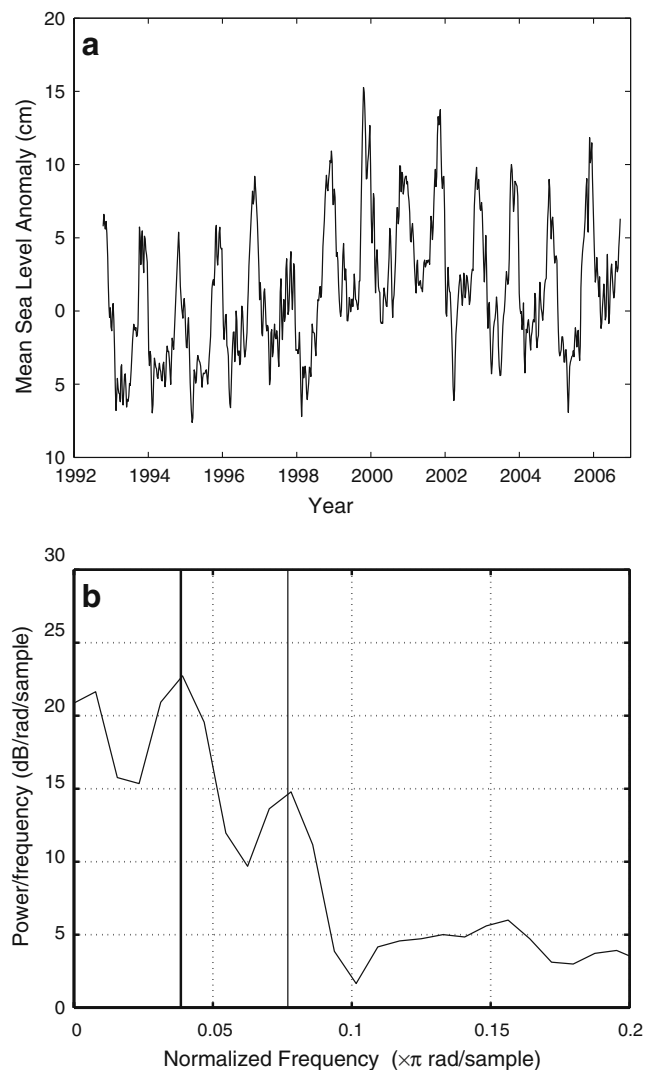


**Fig. 4** **a** Time series of domain-averaged weekly sea-level anomalies (in cm) and **b** the power spectrum density of **a**. The annual (*thick line*) and semi-annual (*thin line*) frequencies are depicted in **b**

patterns of the seasonally reversing basin-scale circulation in the SCS and its regional mesoscale features (the Vietnam dipole eddy and the West Luzon eddy). Their existence seems to be independent of interaction and/or combination of the basin scale and mesoscale modes.

## 4 Interannual and longer-term variability

### 4.1 Altimetric and tide-gauge sea-level variability

We have investigated the interannual and longer-term sea-level variability by examining seasonal-mean sea-level anomalies, after the annual and semi-annual cycles are removed from altimetric data. The seasonal-mean sea-level anomalies are calculated and de-trended by a least-squares analysis.

We have averaged the altimetric seasonal-mean sea-level anomalies available within the  $105\text{--}120^{\circ}$ E and  $5\text{--}25^{\circ}$ N area. The spatially averaged altimetric sea level increased generally from 1993 to 1997 (Fig. 6). An exception was the fall in 1997, followed by an abrupt rebound. After 2002, sea level fell again until the end of 2004. The interannual range (low in 1997/98 and high in 2001/02) was about 15 cm. On average, the altimetric sea level rose at a rate of 0.4 cm/year from 1992 to 2006.

To make a quantitative comparison between altimetric and tide-gauge data, we have considered the period from 1993 to 2001 when both altimetric and tide-gauge were available. Based on the data availability tide-gauge data at S1, S3, S5, S6, and S7 (see Fig. 1) are averaged. The averaged tide-gauge results exhibited similar interannual variations in terms of the magnitude and sequence of significant sea-level change events (Fig. 7). The correlation coefficient for the instantaneous sea-level anomalies is 0.84 between altimetric and tide-gauge measurements, significantly different from zero at the 95% confidence level. Their RMS difference is 3.9 cm. By assuming the errors in the T/P and tide-gauge measurements are uncorrelated, we obtain an estimated RMS error of 2.7 cm. In addition to measurement errors associated with the altimetric and tide-gauge data, the discrepancy may arise from the mismatch of data availability and geographic locations: tide-gauge results are obtained from five stations only; whereas the altimetric results are calculated from many more locations all over the SCS.

For the comparison of the sea-level rise, one must keep in mind that an altimeter measures the geocentric sea level (related to the Earth center), while a tide gauge measures the sea level relative to the local land. From the altimetric data, the mean geocentric rate of the sea-level rise is 1.0 cm/year from 1993 to 2001 (Table 3). The value is more than double that from 1992 to 2006, which implies great

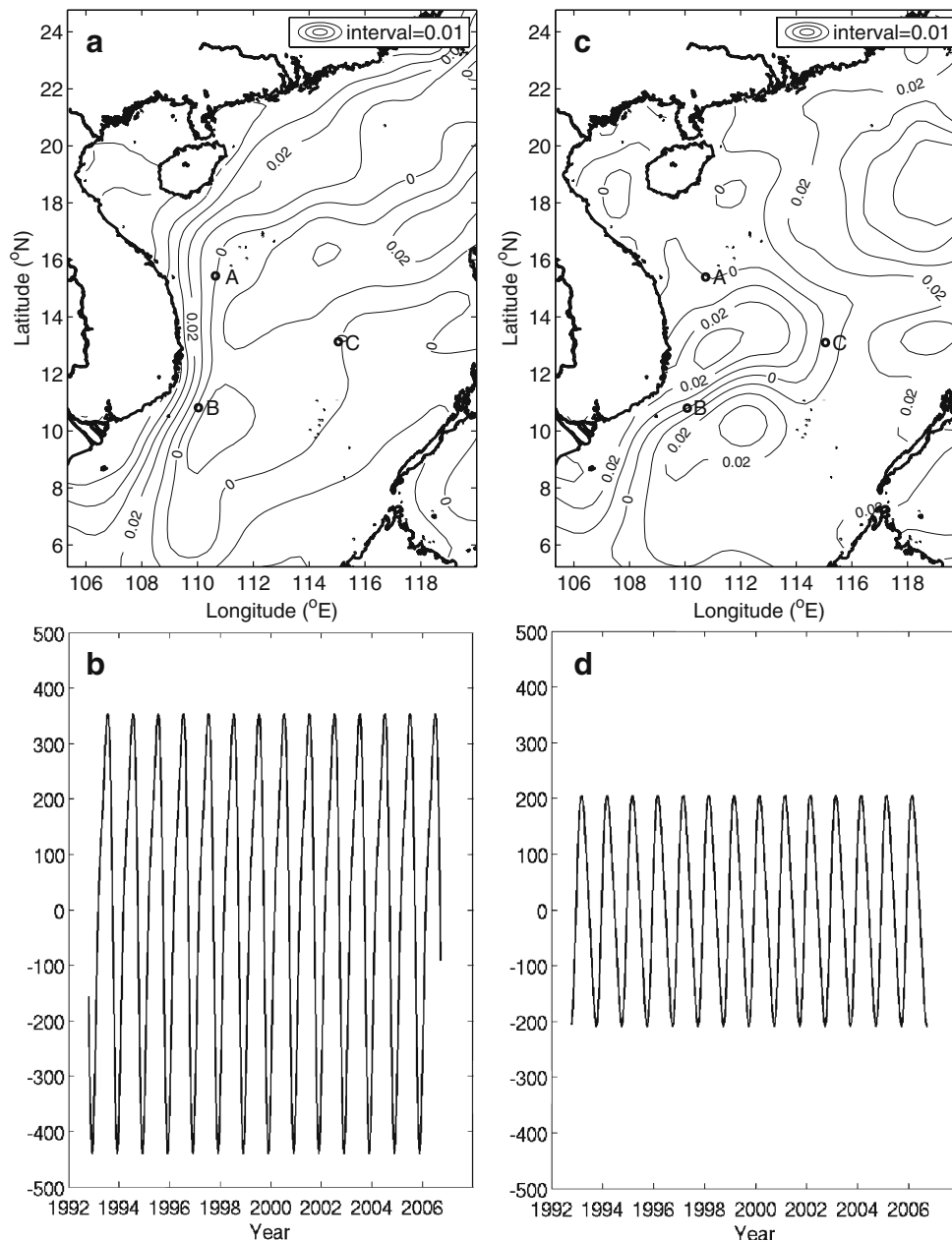


**Fig. 5** EOF modes of the extracted altimetric annual cycle **a** spatial pattern (in cm) of mode 1, **b** time series of mode 1. **c** Spatial pattern (in cm) of mode 2, and **d** time series of mode 2. Three amphidromes A, B, and C are depicted as *open circles* in **a** and **c**

sensitivity of the calculated trend to the data length as a result of the decadal variability. The average sea-level trend observed by the tide gauges is estimated to be a rise of 1.1 cm/year at the five sites from 1993–2001. Taking the vertical movement (subsidence) of the local land (based on a global glacial isostatic adjustment model of Peltier (2004)), the adjusted sea-level rise rate from tide-gauge data is 1.05 cm/year, very close to the altimetric geocentric rate. It is also worth noting that the average rate based on the 1979–2001 tide-gauge data (Fig. 8) is 0.22 cm/year (Table 3) after the model land-subsidence rate being

accounted for, indicating the degree of sensitivity of the calculated rate to the record length as a result of the decadal sea-level variability. Note that sea-level data at S1 and S3 only are used in the averaging.

The regional sea-level rise rate is notably larger than the global-mean rate of 0.28 cm/year based on the altimeter data (Cazenave and Nerem 2004). The rate difference indicates the regional inhomogeneity of the sea-level rise (Han 2002). Han (2002) found the geocentric rate of T/P sea-level rise was essentially zero at Halifax off Atlantic Canada during 1992–2000.

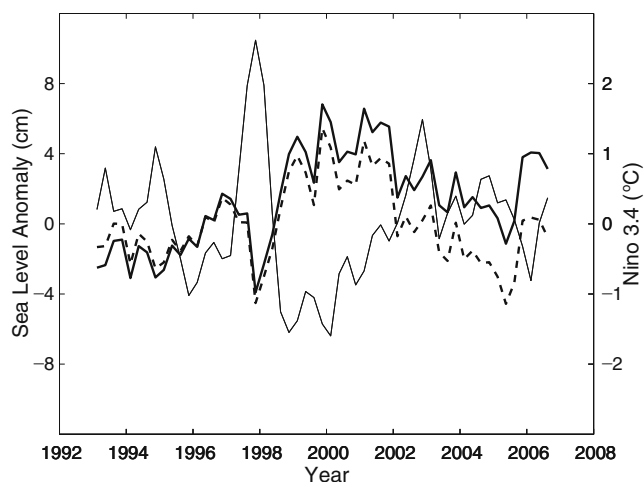


**Fig. 6** Seasonal-mean altimetric sea-level anomalies after the annual and semiannual cycles are removed from 1992 to 2006. The sea-level anomalies (*thick curves*) are shown without (*solid*) and with (*dashed*) de-trending. The Niño 3.4 index (*thin curve*) is also shown

#### 4.2 Steric height variation

We have averaged the seasonal-mean steric height anomalies relative to 700 db for the deep SCS basin (bottom depth >700 m) within the 105–120°E and 5–25°N area. The spatially averaged seasonal-mean steric height anomalies exhibited similar interannual fluctuations to the altimeter and tide-gauge data for the period from 1993 to 2001 (Fig. 9), in both magnitude and time evolution. The correlation coefficient for the instantaneous sea-level anomalies is 0.84 between steric height and altimetric observations and 0.73 between steric height and tide-gauge data, both significantly different from zero at the 95% confidence level. The steric height rise rate of 0.92 cm/year (Table 3) is also close to that revealed by the altimeter data. This agreement suggests that the steric effect can account approximately for the sea-level rise as seen in the altimeter on the basin scale in the 1990s.

Substantial interannual and decadal variability can also be seen in the steric height data for the period from 1979 to 2001. The sea-level rise rate is estimated to be 0.12 cm/year (Table 3), significantly lower than the rate during the 1990s. The rate difference indicates the great sensitivity to the length of record and decadal variability. On the other hand, the steric height rise rate is only about half of the tide-gauge sea-level rate, which suggests that other factors may also play important roles in the long-term sea-level rise in the SCS.

#### 4.3 Relationship with ENSO

The Niño 3.4 index is one of several ENSO indicators based on sea-surface temperatures. Niño 3.4 is the average sea-surface temperature anomaly in the region bounded by

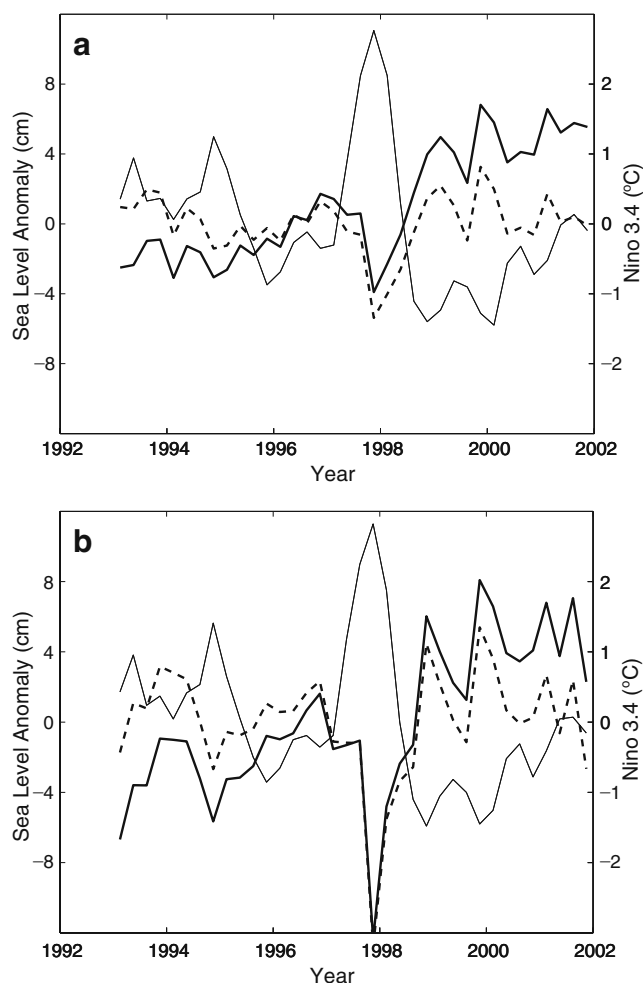


**Fig. 7** Seasonal-mean sea-level anomalies after the annual and semiannual cycles are removed: (a) altimetric observations. (b) Tide-gauge data averaged for the five selected stations. The sea-level anomalies (*thick curves*) are shown without (*solid*) and with (*dashed*) de-trending. The Niño 3.4 index (*thin curve*) is also shown

5°N to 5°S, from 170°W to 120°W. This region has large variability on El Niño time scales, and is close to the area where changes in local sea-surface temperature are important for shifting the large region of rainfall typically located in the far western Pacific. The positive (warm) ENSO is associated with the weakened or reversed trade wind in the equatorial Pacific. In this study, we use the Niño 3.4 index calculated by the Climate Prediction Center of the U.S.

**Table 3** Average sea-level rise rate (cm/year) from altimetric observations, tide-gauge data and steric height for the period from 1993 to 2001 and from 1979 to 2001

|               | 1993–2001 | 1979–2001 |
|---------------|-----------|-----------|
| Altimetry     | 1.0       | N/A       |
| Tide gauge    | 1.05      | 0.22      |
| Steric height | 0.92      | 0.12      |

The altimetric rate has been adjusted for the land subsidence



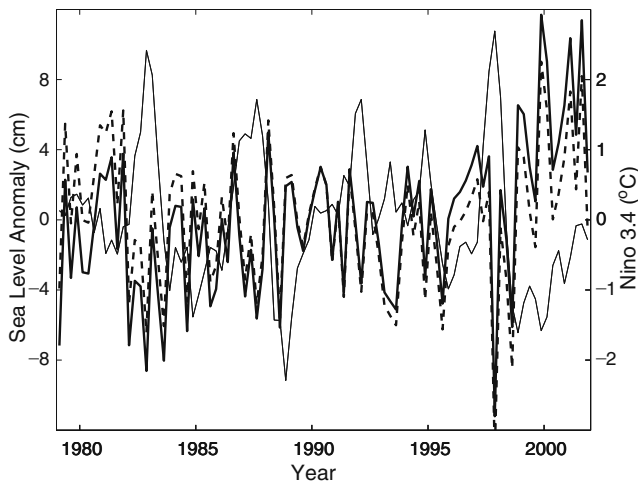


**Fig. 8** Tide-gauge data averaged for the two coastal stations from 1979 to 2001. The sea-level anomalies (*thick curves*) are shown without (*solid*) and with (*dashed*) de-trending. The Niño 3.4 index (*thin curve*) is also shown

National Weather Service (<http://www.cpc.ncep.noaa.gov/data/indices/sstoi.indices>).

There is a clearly defined negative correlation between the sea-level and ENSO index on the interannual scale (Table 4), whether the former is from altimetric observations, tide-gauge data, or steric height and whether the time period is 1993–2001 or 1979–2001. In light of the significant role of the steric height in accounting for the sea-level variability and trend, we now examine the temperature and salinity.

We have averaged the temperature and salinity anomalies in the upper 700-m water column within the 105–120°E and 5–25°N area. There was significant interannual and decadal variability in temperature (Fig. 10) and salinity (Fig. 11) in the SCS for the period from 1979 to 2001.

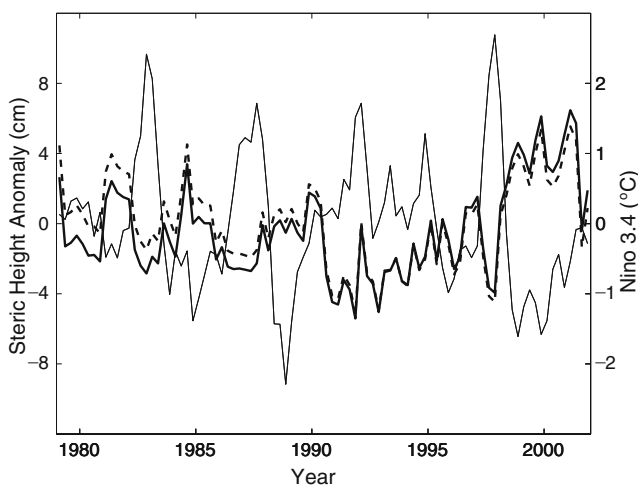


**Fig. 9** Spatially averaged steric height (relative to the 700-m depth) from 1979 to 2001. The sea-level anomalies are shown without (*thick solid*) and with (*thick dashed*) de-trending. The Niño 3.4 index (*thin curve*) is also shown

**Table 4** Correlation coefficient between the Niño 3.4 index and altimetric observations, tide-gauge data or steric height for the period from 1993 to 2001 and from 1979 to 2001

|               | 1993–2001 | 1979–2001 |
|---------------|-----------|-----------|
| Altimetry     | −0.63     | N/A       |
| Tide gauge    | −0.72     | −0.38     |
| Steric height | −0.67     | −0.51     |

Negative correlation (−0.57, significant at the 95% confidence level) was found between the temperature and ENSO (Table 5). The correlation of the salinity with the ENSO was low. The temperature increased at a rate of 0.005°C/year. The salinity decreased at a rate of 0.001 psu/year (Table 6). The increase of temperature and the decrease of salinity lead to the rise of the steric height. For the period from 1993 to 2001, the correlation coefficient with the ENSO was −0.72 for temperature (Table 5). The temperature increase rate was 0.044°C/year and the salinity decrease rate was 0.004 psu/year. The overall contribution to the steric sea-level rise was dominated by the temperature increase. On the interannual scale, the sea-level change seems to be related to the ENSO variability mainly through the temperature variation.

Although a statistical relationship does not seem to exist between the ocean salinity in the upper 700-m water column and the ENSO, the near-surface (from the sea surface to the 50-m depth) salinity (Fig. 11b) is correlated (0.46) with the ENSO (Table 6). On the other hand, the near surface temperature (Fig. 10b) does not show a significant correlation with ENSO (Table 5). The trends (increasing for temperature and decreasing for salinity) for the near-surface layer are larger than those for the upper 700 m (Tables 5 and 6).

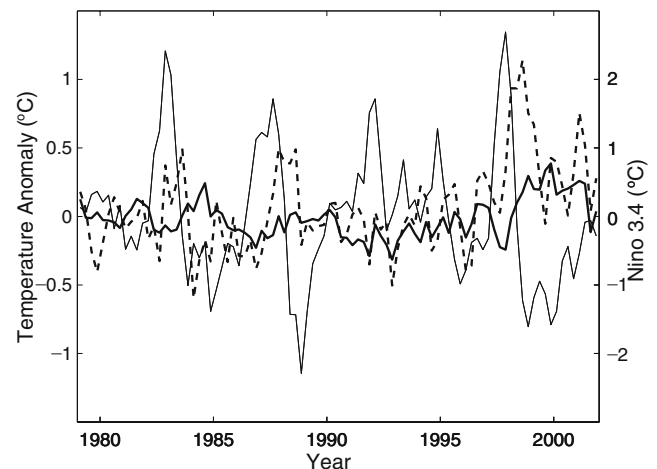


**Fig. 10** Spatially averaged temperature anomalies in the upper 700-m (*thick solid*) and upper 50-m (*thick dashed*) water column from 1979–2001. The Niño 3.4 index (*thin*) is also shown

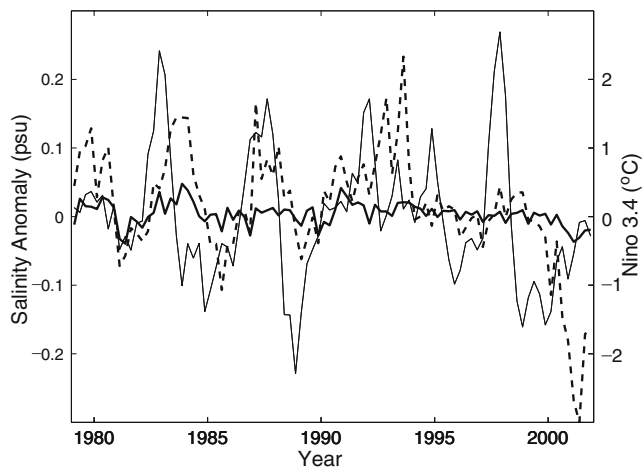


**Fig. 11** Same as Fig. 10 but for salinity

Therefore, the SCS sea-level variability seems to be a manifestation of the ENSO effect through the temperature change in the upper 700-m water column: positive ENSO—low water temperature in the upper 700 m—low sea level in the SCS, and vice versa. Although the sea-level rise is evidently correlated with the temperature increase and salinity decrease, dynamic mechanisms of these changes and whether they are natural decadal variability or a long-term anthropogenic trend remain unclear.

An EOF analysis of altimetric height anomalies after the annual cycle being removed was also carried out. The first mode (Fig. 12) can account for 26% of the total variability. The time series of the first mode clearly shows interannual variability, which is negatively correlated with the Niño 3.4 index. From the first-mode spatial pattern, it is found that the first mode defines the basin-scale circulation in the SCS. The composite of the first mode indicates that the basin-scale SCS circulation tends to be more anticyclonic in El Niño years, that is, weakened cyclonic circulation in winter and/or strengthened anticyclonic circulation in summer.

### 5 Conclusions

We have investigated sea-level variations in the SCS, using the merged altimeter observations (Ducet et al. 2000),

**Table 5** Correlation coefficient between the Niño 3.4 index and temperature for the period from 1993 to 2001 and from 1979 to 2001

|             | 1993–2001     |       | 1979–2001     |       |
|-------------|---------------|-------|---------------|-------|
|             | Correlation   | Rate  | Correlation   | Rate  |
| Upper 700 m | 0.72          | 0.044 | 0.57          | 0.005 |
| Upper 50 m  | Insignificant | 0.072 | Insignificant | 0.021 |

Temperature increase rates (°C/year) are also shown

**Table 6** Correlation coefficient between the Niño 3.4 index and salinity for the period from 1993 to 2001 and from 1979 to 2001

|             | 1993–2001     |       | 1979–2001     |       |
|-------------|---------------|-------|---------------|-------|
|             | Correlation   | Rate  | Correlation   | Rate  |
| Upper 700 m | Insignificant | 0.004 | Insignificant | 0.001 |
| Upper 50 m  | Insignificant | 0.028 | 0.29          | 0.005 |

Salinity decrease rates (psu/year) are also shown

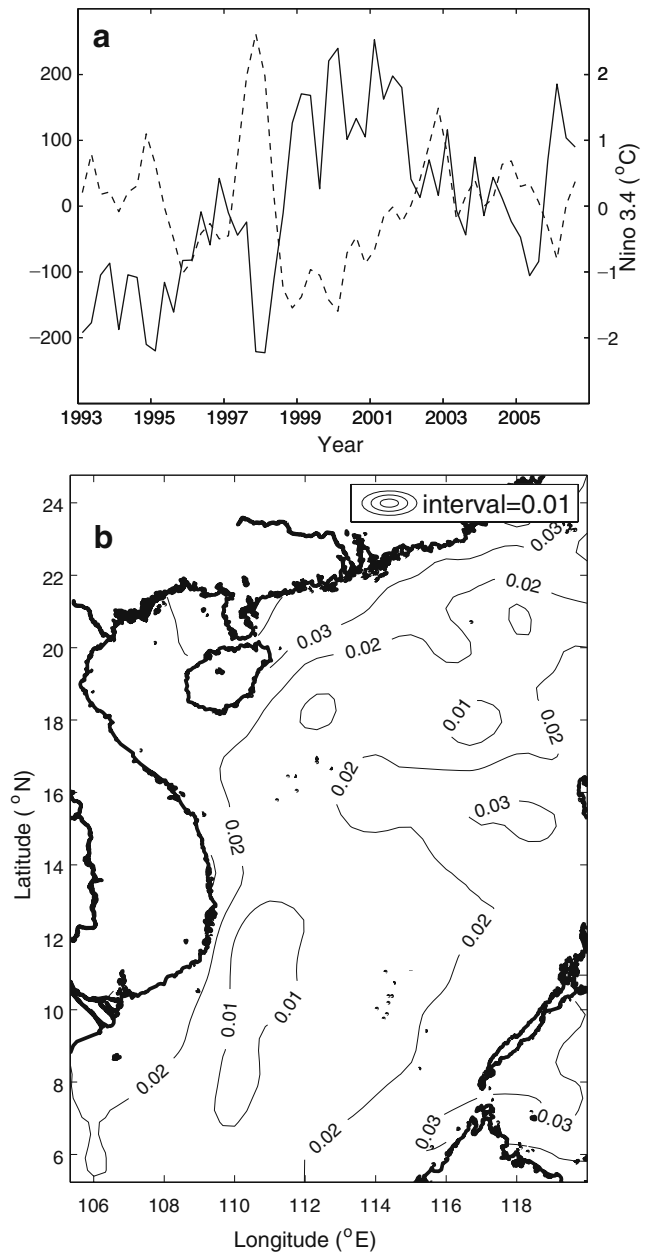


**Fig. 12** a Temporal (dimensionless) and b spatial (in unit of cm) patterns of EOF mode 1 of the altimetric sea-level data in the SCS, after the annual and semiannual cycles are removed. The Niño 3.4 index (dashed) is also shown in a

PSMSL tide-gauge data (<http://www.pol.ac.uk/psmsl>) and temperature and salinity climatology (Ishii et al. 2006). A modified response analysis method is used to remove the aliased residual tidal variability in the altimetric data. Significant annual, interannual, and longer-term sea-level variations are revealed, along with the discussion of their underlying mechanisms and climatic implications.

The present analysis reveals a highly variable spatial distribution of the annual sea-level cycle, from nearly zero in the vicinity of three amphidromic points to over 20 cm. Altimetric sea level is higher in fall/winter in the coastal and shelf seas and in summer/fall in the deep basin, consistent with tide-gauge observations. For the central SCS deeper than 2,000 m, sea level on average has an annual amplitude of 4.5 cm and peaks in August, approximately accounted for by the steric height variation. The reversing monsoon on the seasonal scale is mainly responsible for the basin-scale sea-level depression (dome) in winter (summer), corresponding to the dominant cyclonic (anticyclonic) circulation. Comparisons indicate that the altimetric sea-level results agree well with tide-gauge observations for the annual cycle.

The present study indicates that three annual sea-level amphidromes in the SCS are located where both the dominant basin-scale and the secondary mesoscale features have nil sea-level variation. The amphidromic locations are nearly stationary. The present findings correct Zhang et al.'s (2006) results of four highly unstable amphidromes based on the yearly analyses for 2004 and 2005, respectively. The use of the long data series in our study allows a reliable separation of the annual cycle from the interannual and intra-seasonal variations.

The altimetric sea level from 1992 to 2006 exhibits significant interannual variability, with a range of 15 cm. Similar features are also observed by coastal tide gauges and captured in the steric height relative to 700 db. The altimetric sea-level rise rate is 1.0 cm/year for the period from 1993 to 2001, consistent with the rate derived from coastal tide gauges (1.05 cm/year) and approximately accountable for by the steric height calculated relative to 700 db. The steric height rate of 0.9 cm/year from 1993 to 2001 is much larger than that of 0.12 cm/year for the period from 1979 to 2001. The rate of the coastal tide-gauge sea-level rise also changes from 1.05 cm/year for 1993–2001 to 0.22 cm/year for 1979–2001. The sharp contrast for the two periods implies great sensitivity of the estimated rate to the length of data as a result of the decadal variability.

The present analyses also reveal negative correlation between the sea level in the SCS and the ENSO variability on the interannual time scale. The relationship seems to mainly represent regional manifestation of the ocean temperature change: positive Niño 3.4 index, lower ocean temperature in the upper 700-m water column and lower sea level in the

SCS. However, the sea-level rise is a consequence of both temperature increase and salinity decrease.

**Acknowledgments** The altimeter data were obtained from the AVISO Project. We thank M. Ishii for providing the temperature and salinity climatology. Helpful comments were received from the anonymous reviewers. The work was supported by the National Basic Research Program of China under contract No. 2007CB816003 and the NSFC No. 40676007.

## References

- Cazenave A, Nerem RS (2004) Present-day sea-level change observations and causes. *Rev Geophys* 42:RG3001
- Chang CWJ, Hsu HH, Wu CR, Sheu WJ (2008) Interannual mode of sea level in the South China Sea and the roles of El Niño and El Niño Modoki. *Geophys Res Lett* 35:L03601 doi:10.1029/2007GL032562
- Chen G, Quartly GD (2005) Annual amphidromes: a common feature in the ocean. *IEEE Geosci Remote Sens Lett* 2:423–427
- Chu PC, Chen Y, Lu S (1998) Wind-driven South China Sea deep basin warm-core/cool-core eddies. *J Oceanogr* 54:347–360
- Church J, Gregory JM, Huybrechts P et al (2001) Changes in sea level, in *Climate Change 2001*. In: Houghton JT et al (ed) *The scientific Basis, Contribution of Working Group I to the Third Assessment Report of the Intergovernmental Panel on Climate Change*. Cambridge Univ. Press, New York, pp 639–693
- Ducet N, Le Traon PY, Reverdin G (2000) Global high-resolution mapping of ocean circulation from TOPEX/Poseidon and ERS-1 and -2. *J Geophys Res* 105:19477–19498
- Fang G, Chen H, Wei Z et al (2006) Trends and interannual variability of the South China Sea surface winds, surface height, and surface temperature in the recent decade. *J Geophys Res* 111:C11S16 doi:10.1029/2005JC003276
- Han G (2002) Interannual sea-level variations in the Scotia-Maine region in the 1990s. *Can J Remote Sens* 28:581–587
- Han G (2004) Sea-level and surface current variability in the Gulf of St. Lawrence from satellite altimetry. *Int J Remote Sens* 25:5069–5088
- Han G, Ikeda M, Smith PC (1993) Annual variation of sea surface slopes over the Scotian Shelf and Grand Banks from Geosat altimetry. *Atmos-Ocean* 31:591–615
- Han G, Ikeda M, Smith PC (1996) Oceanic tides on the Newfoundland and Scotian Shelves from TOPEX/POSEIDON altimetry. *Atmos-Ocean* 34:589–604
- Han G, Tang CL, Smith PC (2002) Annual variations of sea surface elevations and currents over the Scotian Shelf and Slope. *J Phys Oceanogr* 32:1794–1810
- Ishii M, Kimoto M, Sakamoto K et al (2006) Steric sea-level changes estimated from historical ocean subsurface temperature and salinity analyses. *J Oceanogr* 62:155–170
- Morimoto A, Yoshimoto KY, Yanagi T (2000) Characteristics of sea surface circulation and eddy field in the South China Sea revealed by satellite altimetric data. *J Oceanogr* 56:331–344
- Peltier WR (2004) Global glacial isostasy and the surface of the Ice-Age Earth: the ICE-5G(VM2) model and GRACE. *Ann Rev Earth Planet Sci* 32:111–149
- Qu T (2000) Upper layer circulation in the South China Sea. *J Phys Oceanogr* 30:1450–1460
- Shaw PT, Chao SY (1994) Surface circulation in the South China Sea. *Deep Sea Res I* 41:1663–1683

- Shaw PT, Chao SY, Fu LL (1999) Sea surface height variation in the South China Sea from satellite altimetry. *Oceanol Acta* 22:1–17
- Wang GH, Su JL, Chu PC (2003) Mesoscale eddies in the South China Sea observed with altimetry. *Geophysical Res Lett*. doi: [10.1029/2003GL018532](https://doi.org/10.1029/2003GL018532)
- Wang Y, Fang G, Wei Z et al (2006a) Interannual variation of the South China Sea circulation and its relation to El Niño, as seen from a variable grid global ocean model. *J Geophys Res* 111: C11S14 doi:[10.1029/2005JC003269](https://doi.org/10.1029/2005JC003269)
- Wang G, Chen D, Su J (2006b) Generation and life cycle of the dipole in the South China Sea summer circulation. *J Geophys Res*. doi:[10.1029/2005JC003314](https://doi.org/10.1029/2005JC003314)
- Wang G, Chen D, Su J (2008) Winter eddy genesis in the eastern South China Sea due to orographic wind-jets. *J Phys Oceanogr* 38:726–732
- Wu CR, Chang CWJ (2005) Interannual variability of the South China Sea in a data assimilation model. *Geophys Res Lett* 32:L17611 doi:[10.1029/2005GL023798](https://doi.org/10.1029/2005GL023798)
- Yanagi T, Takao T, Morimoto A (1997) Co-tidal and co-range charts in the South China Sea from satellite altimetry. *Lar Mer* 35:85–93
- Zhang C, Wang B, Chen G (2006) Annual sea-level amphidromes in the South China Sea revealed by merged altimeter data. *Geophys Res Lett*. doi:[10.1029/2006GL026493](https://doi.org/10.1029/2006GL026493)